



## Cooperatively Generated Stresslet Flows Supply Fresh Fluid to Multicellular Choanoflagellate Colonies

Marcus Roper,<sup>1,\*</sup> Mark J. Dayel,<sup>2</sup> Rachel E. Pepper,<sup>3,4</sup> and M. A. R. Koehl<sup>3</sup>

<sup>1</sup>*Department of Mathematics, University of California, Los Angeles, California 90095, USA*

<sup>2</sup>*Molecular and Cellular Biology, University of California, Berkeley, California 94720, USA*

<sup>3</sup>*Integrative Biology, University of California, Berkeley, California 94720, USA*

<sup>4</sup>*Civil and Environmental Engineering, University of California, Berkeley, California 94720, USA*

(Received 1 March 2013; published 31 May 2013)

The flagellated protozoan *Salpingoeca rosetta* is one of the closest relatives of multicellular animals. Unicellular *S. rosetta* can be induced to form multicellular colonies, but colonies swim more slowly than individual cells so the advantages conferred by colony formation are uncertain. Here we use theoretical models to show that hydrodynamic cooperation between cells can increase the fluid supply to the colony, an important predictor of feeding rate. Our results suggest that hydrodynamic benefits may have been an important selective factor in the evolution of early multicellular animals.

DOI: 10.1103/PhysRevLett.110.228104

PACS numbers: 47.63.-b, 87.16.Qp, 87.18.Fx

The choanoflagellate *Salpingoeca rosetta* uses a single whiplike flagellum to drive a flow of water and captures bacterial prey from the flow on a collar of microvilli. Although unicellular under many growth conditions, *S. rosetta* cultures maintained in log phase growth produce chainlike colonies bound together by extracellular matrix and cell-cell bridges [1,2] (Fig. 1). Cells in colonies remain undifferentiated and divide autonomously. Because of *S. rosetta*'s phylogenetic position, and because its colonies lack many of the features of derived multicellularity, they are thought to share features in common with the progenitors of multicellular animals. Understanding the selective advantages of the colonial form may therefore reveal evolutionary and ecological forces that shaped the first origins of animal multicellularity.

The cooperative hydrodynamics of *S. rosetta* colonies cannot be described by existing theory for cooperative feeding. Using the Volvocales (a family of hollow spherical algal colonies) as a model system, Short *et al.* [3] showed colonies of flagellated cells benefit from increased nutrient uptake. The cells along the periphery of *Volvox* spp. colonies beat in a coordinated anterior-posterior direction to create an effective uniform propulsive stress,  $\sigma_s$  along the colony surface. The total propulsive force is balanced by viscous drag  $\sim \eta R U_{\text{swim}}$ , with  $\eta$  the viscosity of the surrounding fluid,  $R$  the colony radius, and  $U_{\text{swim}}$  swimming speed. If  $\sigma_s$  is conserved between colonies of different sizes, then  $U_{\text{swim}} \sim \sigma_s R / \eta$ , so larger colonies swim faster and encounter more dissolved molecules or prey organisms per unit time.

By contrast, in colonial *S. rosetta* we find no evidence that flagellar phases, frequencies, or axes are coordinated (See Supplemental Material and Supplemental Movie 1 [4]). Because flagella of different cells “push” in different directions, forces from different parts of the colony tend to cancel and colonies swim more slowly and should feed less

well than single cells. Here we identify another possible mechanism of hydrodynamic cooperation, showing that the anisotropically distributed cells of a colony create long range feeding flows, and draw in a larger volume flux of fluid per cell than cells can individually. Remarkably, slower swimming augments, rather than diminishes, the rate at which colonies draw in fluid.

*S. rosetta* prey encounter rates depend both on the speed of swimming of the organism and upon the dynamics of their flagella-created feeding flows. Typical flow Reynolds numbers are  $\approx 10^{-4}$  [5], so viscous stresses are manyfold larger than inertial stresses [6]. The flow is therefore governed by Stokes' equations, and can be described completely by superposition of singularities, representing the action of point forces and sources [7].

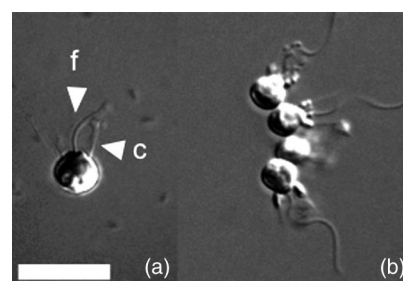


FIG. 1. Multi- and unicellular stages in the life history of *S. rosetta*. (a) Under a broad variety of growth conditions, cells are planktonic and either freely swimming or attached to substrates. A flagellum (f) propels freely swimming cells through water and creates flows from which prey are captured on a collar of microvilli (c). (b) When maintained in log phase, incomplete scission during cell division produces chainlike colonies. Not shown: When grown with the bacterium *Algoriphagus machopogensis*, cells make compact rosette colonies (see Supplemental Material [4]). Scale bar: 10  $\mu\text{m}$ .

*A single point force accurately represents sessile choanoflagellate feeding flows.*—We used particle tracking [8] to analyze bacterial trajectories from videos (captured at 1 frame/s) of the flow produced by sessile (and therefore stationary) thecate *S. rosetta* cells anchored to cover slides [Fig. 2(a)]. We follow [5] by modeling the feeding flow as a constant point force,  $F_p$ , a distance  $h$  above the cover slide, treated as an infinite planar surface [9]. We matched  $F_p$  and  $h$  from (i) the flow field,  $\mathbf{u}$ , far from the cell and (ii) the distance between cover slide and the stagnation points. We found  $F_p \equiv 2.4 \pm 0.8$  pN and that the point force is located  $16.8 \pm 2.5 \mu\text{m}$  above the cell apex, coinciding approximately with the the flagellum tip. Although tailored to the far field velocities, this simplified model also quantitatively produces the velocity field close to the cell except near the base of the flagellum where neglect of the distributed flagellar force leads velocities to be underestimated [Fig. 2(a)].

Neglecting buoyancy, freely swimming cells exert no net force on the surrounding fluid so the propulsive force

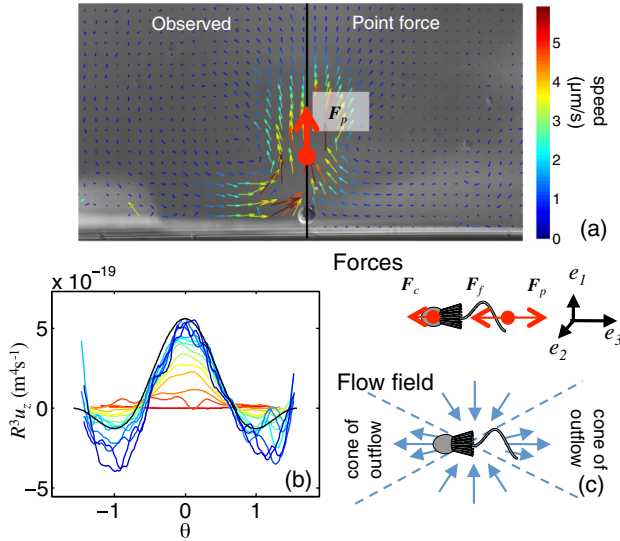


FIG. 2 (color online). Mapping and modeling feeding flows created by single *S. rosetta* cells. (a) Left panel: experimentally measured velocity field for a single thecate cell. 49000 bacterial velocity measurements were interpolated to a regularly spaced grid of  $x$ ,  $y$  points and then averaged over time. Arrows give displacements in 1 s and are also color-coded by speed. Right panel: Flow field vectors from a point force model match the velocity field except adjacent to the cell body. (b) To determine the total flagellum force we match the measured velocity field far from the cell to the asymptotic form of the point force flow field. Colors: scaled velocity field  $R^3 u_z$  on arcs of different radius (equispaced from red:  $R = 12 \mu\text{m}$  to blue:  $R = 74 \mu\text{m}$ ),  $R$ , parametrized by polar angle  $\theta$ . Black: theoretical velocity. (c) Upper panel: For a freely swimming cell, propulsive ( $F_p$ ) and drag forces ( $F_f$ ,  $F_c$ ) create a stresslet with principal axes  $\{\mathbf{e}_i\}$  (upper panel), with cones of outflow (blue velocity arrows) fore and aft of the cell and inflow around the cell equator (lower panel).

$F_p$  is balanced by drag forces on the cell body,  $\mathbf{F}_c$ , and flagellum,  $\mathbf{F}_f$  [10]. We model these contributions by point forces located at  $\mathbf{r}_p$ ,  $\mathbf{r}_c$ , and  $\mathbf{r}_f$  respectively [Fig. 2(c)], identifying  $\mathbf{r}_c$  with the center of the cell body, and  $\mathbf{r}_f = \mathbf{r}_p$  as the flagellum tip. Then, at a point  $\mathbf{r}$ , far from the cell, the forces resolve into the stresslet flow field  $\mathbf{u} = -[3(\mathbf{r} \cdot \mathbf{S} \cdot \mathbf{r})\mathbf{r}/8\pi\eta r^5]$ , where

$$\mathbf{S} = - \sum_{i \in \{p, c, f\}} \left[ \frac{1}{2}(\mathbf{F}_i \mathbf{r}_i + \mathbf{r}_i \mathbf{F}_i) - \frac{1}{3}(\mathbf{r}_i \cdot \mathbf{F}_i) \mathbf{1} \right], \quad (1)$$

( $\mathbf{1}$  is the identity tensor). We estimate the drag forces by resistive force theory [11]. Specifically, if  $\mathbf{U}$  is the swimming speed and  $\mathbf{n} = (\mathbf{r}_f - \mathbf{r}_c)/\|\mathbf{r}_f - \mathbf{r}_c\|$  is a unit vector in the direction of the flagellum, then  $\mathbf{F}_c = 6\pi d\eta \mathbf{U}$  ( $d = 2.4 \mu\text{m}$  is the radius of the cell) and  $\mathbf{F}_f = (Z_{\parallel} - Z_{\perp})(\mathbf{U} \cdot \mathbf{n})\mathbf{n} + Z_{\perp} \mathbf{U}$  (see Supplemental Material [4] for derivation of the drag coefficients  $Z_{\parallel}$  and  $Z_{\perp}$ ). Balance of forces,  $\sum_{i \in \{p, c, f\}} \mathbf{F}_i = \mathbf{0}$ , then yields  $\mathbf{U} = (F_f/(6\pi\eta d + Z_{\parallel})) = 28 \mu\text{m s}^{-1}$  comparable with measured swimming speeds [12] and also the values of the forces  $\mathbf{F}_{c,f}$ .

*The stresslet flow continuously supplies fresh fluid, undepleted of prey bacteria, to the cell.*—The stresslet tensor  $\mathbf{S}$  is symmetric and traceless so it can be diagonalized by an orthonormal basis of eigenvectors,  $\{\mathbf{e}_i\}$   $i = 1, 2, 3$ , with eigenvalues  $\lambda_i$ :  $\sum_i \lambda_i = 0$ . Two of the eigenvalues,  $\lambda_1$  and  $\lambda_2$  say, must have the same sign. If  $\lambda_3 > 0$ , there is radial inflow inside of a pair of elliptical cones with axes on  $\pm \mathbf{e}_3$  and radial outflow outside of these cones. Flow in the two regions is reversed if  $\lambda_3 < 0$ . Assuming  $|\lambda_1| \geq |\lambda_2|$  we can compute the fluid flux over any surface enclosing the swimmer to obtain the rate of fluid supply through the cones of inflow,

$$f = \frac{|\lambda_1|^{5/2}}{3\pi\eta|\lambda_1 - \lambda_3|^{3/2}} \left| M_{5/2,3/2} - 3\left(1 - \frac{\lambda_3}{\lambda_1}\right)M_{3/2,1/2} - \frac{\lambda_3}{\lambda_1}M_{3/2,3/2} \right|, \quad (2)$$

where  $M_{p,q} \equiv \int_0^{\pi/2} ((1 - r\sin^2\phi)^p / (1 - s\sin^2\phi)^q) d\phi$  for  $r \equiv ((\lambda_1 - \lambda_2)/\lambda_1)$ ,  $s \equiv ((\lambda_1 - \lambda_2)/(\lambda_1 - \lambda_3))$  (see Supplemental Material [4] for more details). Though the terms in (2) must in general be evaluated by numerical quadrature, if (i)  $|\lambda_1| \gg |\lambda_2|$  then  $f \sim (|\lambda_1|/\pi\eta)$  or (ii)  $\lambda_1 \approx \lambda_2$  then  $f \sim (|\lambda_1|/3^{1/2}\pi\eta)$ . In general the flux to the cell increases in proportion to the largest eigenvalue of  $\mathbf{S}$ , i.e., increases with the size of the forces or their separation.

If cells swim at velocity  $\mathbf{U}$  then fluid is also advected to the cell at rate  $f_{\text{adv}} = \pi R^2 U$ , where  $R$  is the radius of a spherical control surface. For a single swimming cell the modeled values of  $f$  and  $U$  give  $f_{\text{adv}}/f = 0.02R^2$ , if  $R$  is measured in  $\mu\text{m}$ . Thus at large distances, advection dominates but within  $\sim 7 \mu\text{m}$  of the cell, transport is dominated by the stresslet flow: swimming faster does not increase the

total flux (see Supplemental Material [4]). Colonies will be shown to swim more slowly and have larger stresslet eigenvalues, so the stresslet flow field dominates up to even greater distances.

*Pairs of choanoflagellate cells anchored together can access a greater volume of new fluid per unit time than freely-swimming cells.*—We modified our model to include the effect of two cells swimming together: Cell dimers are developmental and evolutionary intermediates between individual cells and chainlike colonies. Dimer configurations are specified by three angles:  $\theta_1$  is the smallest angle between the flagellum of the first cell and the normal to the axis joining the two cell centers and  $(\theta_2, \phi_2)$  are the spherical polar angles of the second flagellum relative to the normal vector [Fig. 3(a)].  $(\theta_1, \theta_2, \phi_2)$  are set during cell division by the position of the cell-cell bridge and direction of the polarity axis of the daughter cell. A cell dimer is associated with 6 point forces,  $\{F_i^j : i \in \{p, c, f\}, j \in \{1, 2\}\}$  [Fig. 3(b)]. For any general arrangement of these forces, the dimer will rotate with angular

velocity  $\boldsymbol{\Omega}$  and will swim with velocity  $\mathbf{U}$ , determined by the condition that the dimer be force and torque free. For each pair  $(\theta_1, \theta_2)$ , we determine  $\phi_2$  to maximize  $f$  [Fig. 3(c)].

The flowerlike shape of the  $(\theta_1, \theta_2, f)$  surface reveals two locally optimal configurations for a pair of cells; pole-to-pole or side-by-side [Fig. 3(c)] with fluid fluxes per cell that are respectively  $2.17 \times$  larger and identical to freely swimming cells. Pole-to-pole configurations increase the stresslet eigenvalues for the following two reasons: First, slower swimming [Fig. 3(c)] increases the flagellar force  $\mathbf{F}_p^i + \mathbf{F}_f^i$  by reducing the drag forces acting on individual flagella, mimicking the observed increase in fluid transport by the flagellum of a cell prevented from swimming [13,14]. Second, the separation of the two flagellar forces  $\mathbf{F}_p^{\{1,2\}}$  is maximized.

*We extended our calculations to chainlike colonies of more than two cells.*—If cells independently regulate their positions, then  $N$  cells have  $4N - 5$  configurational degrees of freedom. However, tuning of these parameters during colony morphogenesis requires information to be propagated between cells, since the division of any cell alters the position of all of the other cells within the chain. We therefore apply a simple morphogenetic model: For  $i = 1, 2, \dots, N - 1$ , we use the landmarks of the cell  $i$  [flagellum direction  $\mathbf{n}_i$ , displacement  $\mathbf{r}_c^i - \mathbf{r}_c^{i-1}$  from cell  $(i - 1)$ ] to define coordinate axes. We require that each cell division be identical: i.e., the coordinates of the flagellum vector  $\mathbf{n}_{i+1}$  and displacement  $\mathbf{r}_c^{i+1} - \mathbf{r}_c^i$  of the  $(i + 1)$ th cell be independent of  $i$  with respect to these axes. This model has the advantage that any cell-division occurring in a  $N$ -cell colony produces the same  $N + 1$  cell colony, independently of which cell divided. Chains formed by this rule are helices with constant curvature and torsion. The four degrees of freedom in cell position and orientation dictate the curvature  $\kappa$  and torsion  $\tau$  of the helix and the flagella angles relative to the tangent, normal and binormal of the helix. Given  $N$ ,  $\kappa$ , and  $\tau$  we choose the orientational angles of the flagella in the colony to optimize  $f$  [Figs. 4(a)–4(c)]. When  $N = 3$ , the optimal configuration has  $(\kappa, \tau) = (1/d, 1/d)$ , the largest values compatible with the finite size of cells: cells are stacked almost side by side, their flagella lying in parallel planes and pointing toward the vertices of an equilateral triangle, per-cell fluid supply is 75% greater than for freely-swimming cells [Fig. 4(a)]. As  $N$  increases, the optimal helix becomes a semi-circular arc with flagella pointing radially outward [Figs. 4(a)–4(c)], similar to real *S. rosetta* colonies [Fig. 1(b)].

Do the volume fluxes increase in proportion to the number of cells in the chain? We analyzed the fluid supply to a large semicircle of  $N$  cells (see Supplemental Material [4] for detailed calculations), and found using real *S. rosetta* dimensions that  $f \sim 65N^2 \mu\text{m}^3 \text{s}^{-1}$ , increasing faster than the colony's metabolic needs ( $\sim N$ ).

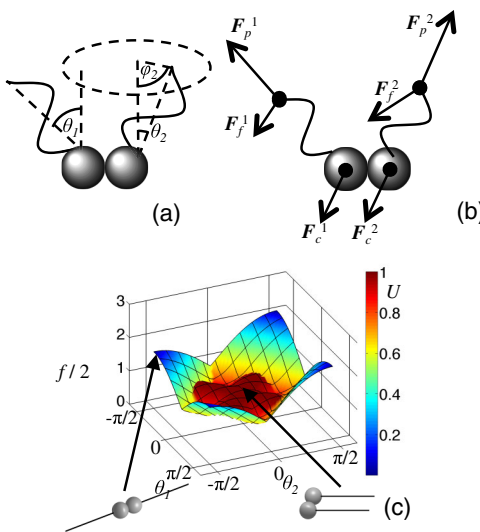


FIG. 3 (color online). Enhanced feeding in dimers of *S. rosetta* cells. (a) We measured how the volume flux of fluid to the cells in the dimer,  $f$ , depends upon the orientations of the two cells, parametrized by angles  $(\theta_1, \theta_2, \phi_2)$ . (b) To compute the feeding flux, we balance the propulsive forces  $\mathbf{F}_p^{1,2}$  from the two cells with drag forces  $\mathbf{F}_{c,f}^{1,2}$  from the cell bodies and flagella. To do this we must also obtain the swimming and rotational velocities  $(\mathbf{U}, \boldsymbol{\Omega})$  of the cell dimer. (c) Feeding flux for different configurations of cells. Here we vary  $(\theta_1, \theta_2)$  and for each such pair of angles select the value of  $\phi_2$  to maximize  $f$ .  $f$  is nondimensionalized by  $f_{\text{single}}$ , flux for a single freely swimming cell;  $f/2 > 1$  means that the volume flux per cell is greater than for freely swimming cells. Surface-coloring shows the swimming speed of the dimer  $U$ , nondimensionalized by the swimming speed of a single cell. Pole-to-pole  $(\theta_1, \theta_2) = (\pm\pi/2, \pm\pi/2)$  and side-by-side  $(\theta_1, \theta_2) = (0, 0)$  configurations are shown.

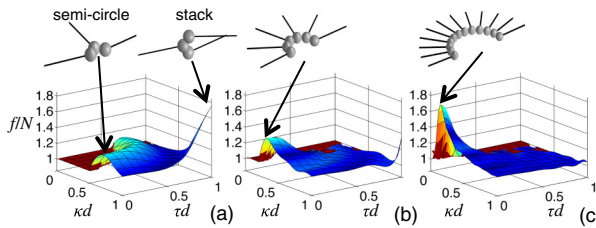


FIG. 4 (color online). Optimal helical cell configurations. (a) For three cells, the optimal helix is a stack, while an additional, local optimum is formed from a semicircular arc of cells with flagella pointing in an outward radial direction. (b), (c) For  $N = 6$  and  $N = 12$  cells the semicircular arc becomes the optimal helix. Color scale same as Fig. 3(c).

We measured the angles between the axes of neighboring cells in real choanoflagellate colonies [Fig. 5(a)].—Average cell-cell angles were relatively conserved between colonies (mean:  $0.60 \pm 0.17$  rads for *S. rosetta*). Although intracolony variation in cell-cell angles (mean: 0.22 radians) reduces  $f/N$ , the variation is small enough that  $f/N > 1$  (see Supplemental Material [4]). Mean cell-cell angles did not depend on colony size, suggesting that chains conserve their curvature during growth. Although  $f/N > 1$  for each colony, most observed colonies were far from the optimal helical geometry for their size [Fig. 5(a)]. Hypothesizing that fixing cell-cell angles would produce suboptimal values of  $f/N$  at some stage in colony development, we simulated growth of a colony with  $N = 12$  cells. We chose cell-cell angles to maximize  $f$  for  $N = 12$ . Intermediate colonies with these cell-cell angles have smaller per-cell fluid supply  $f/N$  [Fig. 5(b)] than colonies with optimal helical geometry. In fact, over most of its development (for  $N < 8$ )  $f/N < 1$ , so colonies fed worse even than single cells. Colonies grown beyond 12 cells did relatively less well than the optimal helical colonies for each cell number [Fig. 5(b)]. These data suggest that cell-cell angles in real colonies may be constrained by trade-offs between maximizing feeding rates at earlier and later growth stages.

Our modeling predictions suggest that cooperative hydrodynamics may offer a competitive advantage to modern colonial choanoflagellates and the early metazoans they are believed to resemble [15]. Decreased drag forces upon flagella and greater spatial separation of flagella forces increase the colony stresslet and its supply of fresh fluid. If enhanced feeding by cooperative hydrodynamics were an evolutionary force toward multicellularity, there are constraints on the configurations and numbers of cells involved. However, we also find that a simple morphogenetic model is sufficient to produce such configurations without requiring cell-cell communication or coordination of flagellar beating.

Although fresh fluid supply provides an upper bound upon the rate at which prey is drawn to the colony and is a common proxy for feeding rate [13,16], colonies of

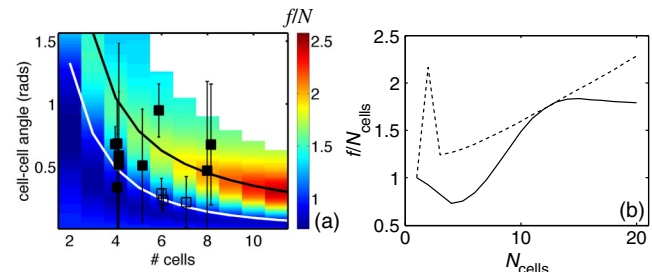


FIG. 5 (color online). (a) Cell-cell angles measured from real chain colonies of *S. rosetta* (closed squares) cultured and imaged using standard techniques [2], and *Desmarella* cf. *moniliformis* (open squares) [20]. Error bars: s.d. Cell numbers are slightly displaced from integer values for clarity. Heat map gives the predicted per-cell flux  $f/N$ . White line: minimum cell-cell angle for  $f/N > 1$ , grey line: optimal cell-cell angle for a semicircular colony. (b) We simulated feeding by developmental precursors of a colony with  $N = 12$  cells (solid curve). Intermediate-sized colonies feed less well even than freely swimming cells ( $f/N < 1$  for  $N < 8$ ), and much worse than semicircular colonies (dashed curve).

different sizes and freely-swimming single cells may differ in their abilities to remove prey from these flow fields. Full validation of the model will require either direct imaging [17] or simulations [18] of prey capture by both single and colonial cells.

*Why does *S. rosetta* have unicellular as well as multicellular forms?*—Real prey distributions are patchy [19] and successful flagellar feeders must forage for and exploit prey patches. Colonies swim more slowly than single cells so are disadvantaged moving between prey patches. Since colony formation is triggered when cells are maintained with high concentrations of bacterial prey we hypothesize that colonies may be a transient life-phase triggered when *S. rosetta* cells find themselves in persistent patches.

We gratefully acknowledge financial support from the Alfred P. Sloan Foundation (M.R.), from the Miller Institute for Basic Research (M. R., M. J. D. and R. E. P.), and from the National Science Foundation (Grant No. IOS-1147215) to M. A. R. K. We thank N. King for discussions.

\*mroper@math.ucla.edu

- [1] S. Fairclough, M. Dayel, and N. King, *Curr. Biol.* **20**, R875 (2010).
- [2] M. J. Dayel, R. A. Alegado, S. R. Fairclough, T. C. Levin, S. A. Nichols, K. McDonald, and N. King, *Dev. Biol.* **357**, 73 (2011).
- [3] M. Short, C. Solari, S. Ganguly, T. Powers, J. Kessler, and R. Goldstein, *Proc. Natl. Acad. Sci. U.S.A.* **103**, 8315 (2006).
- [4] See Supplemental Material at <http://link.aps.org/supplemental/10.1103/PhysRevLett.110.228104> for images of rosette colonies, resistive force calculations and analysis of the effect of prey diffusion, colony swimming and noisy cell placement on feeding rates.

- [5] M. Pettitt, B. Orme, J. Blake, and B. Leadbeater, *Eur. J. Protistol.* **38**, 313 (2002).
- [6] E. Purcell, *Am. J. Phys.* **45**, 3 (1977).
- [7] S. Kim and S. J. Karrila, *Microhydrodynamics: Principles and Selected Applications* (Butterworth-Heinemann, London, 1991).
- [8] J. Crocker and D. Grier, *J. Colloid Interface Sci.* **179**, 298 (1996); M. Roper, A. Simonin, P. Hickey, A. Leeder, and N. Glass (to be published).
- [9] J. Blake, *Proc. Cambridge Philos. Soc.* **70**, 303 (1971).
- [10] T. Pedley and J. Kessler, *Annu. Rev. Fluid Mech.* **24**, 313 (1992); K. Drescher, J. Dunkel, L. H. Cisneros, S. Ganguly, and R. E. Goldstein, *Proc. Natl. Acad. Sci. U.S.A.* **108**, 10940 (2011).
- [11] J. Gray and G. Hancock, *J. Exp. Biol.* **32**, 802 (1955); C. Brennen and H. Winet, *Annu. Rev. Fluid Mech.* **9**, 339 (1977); M. Roper, R. Dreyfus, J. Baudry, M. Fermigier, J. Bibette, and H. A. Stone, *J. Fluid Mech.* **554**, 167 (2006).
- [12] M. Koehl, N. King, and R. Stocker (unpublished).
- [13] K. Christensen-Dalsgaard and T. Fenchel, *Aquatic Microbial Ecology* **33**, 77 (2003).
- [14] J. Lighthill, *SIAM Rev.* **18**, 161 (1976).
- [15] N. King, *Dev. Cell* **7**, 313 (2004).
- [16] S. Childress, M. Koehl, and M. Miksis, *J. Fluid Mech.* **177**, 407 (1987).
- [17] T. Fenchel, *Limnol. Oceanogr.* **25**, 733 (1980).
- [18] L. Fauci, *American Zoologist* **36**, 599 (1996).
- [19] J. P. Barry and P. K. Dayton, in *Ecological Heterogeneity, Ecological Studies*, edited by J. Kolasa and S. Pickett (Springer, New York, 1991), Vol. 86, p. 270.
- [20] See the Encyclopedia of Life at <http://www.eol.org>.